CrossMark

Improved longtime stability of highly efficient polymer solar cells by accurately self-formed metal oxide interlayer at metal electrode

Xiangkun Jia[a], Jianping Zhou[b,*], Sumei Huang[a], Wei Ou-Yang[a], Zhuo Sun[a], Xiaohong Chen[a,*]

[a] Engineering Research Center for Nanophotonics & Advanced Instrument, Ministry of Education, School of Physics and Materials Science, East China Normal University, Shanghai 200062, China
[b] School of Automation Engineering, Shanghai University of Electric Power, Shanghai 200090, China

ARTICLE INFO

ABSTRACT

Al as a cheap and air-stable metal material has been widely applied to polymer solar cells (PSCs) as an efficient electrode. However, there are few care whether Al is a right electrode in PSCs for longtime stability. The inverted PSCs with the structure of ITO/ZnO/PTB7-Th:PC$_{71}$BM/MoO$_3$/Metal electrode were fabricated and the performance and stability of inverted PSCs with Al and AgAl electrodes were investigated. PSCs with AgAl electrode got the highest PCE value of 9.3% without aging. While the PCE of PSCs with Al electrode can be gradually improved and reach the highest value of 7.8% after aging for 36 h, which is attributed to the formation of AlO$_x$ interlayer at the interface of MoO$_3$/Al. PSCs with AgAl electrode still retained 69% of the initial PCE value and got 6.6% of PCE aging for 796 days, showing amazing stability. However, PSCs with Al electrode was dropped to 3.7% of PCE aging for 796 days due to the continuously increased thickness of AlO$_x$ interlayer, which can greatly increase the series resistance of cells. PSCs with AgAl electrode can be further improved and reach 10.2% of PCE using AZO (Al doped ZnO) instead of ZnO and show better UV-light resistance. The enhanced stability of PSCs with AgAl electrode is attributed to the dense and limited thick AlO$_x$ interlayer self-formed at the MoO$_3$/AgAl interface due to the low content of Al. Our results demonstrated that Ag alloy electrode such as AgAl is a good strategy to accurately control the thickness of the metal oxidation interlayer, which can overcome the disadvantage of Al electrode and greatly improve the longtime stability of devices.

1. Introduction

Polymer solar cells (PSCs) has experienced a progressive development in recent ten years, the power conversion efficiency (PCE) of single junction PSCs has increased over 10% (Jia et al., 2016; Liu et al., 2015; Zhao et al., 2016, 2017). The great progress in low band gap polymer with deep highest occupied molecular orbital (HOMO) energy level contributes to improve open circuit voltage (V$_{OC}$) and the short circuit photocurrent (J$_{SC}$) of PSCs (An et al., 2013; Liao et al., 2013). Other efficient approaches, such as optimizing the film nanoscale morphology (Huang et al., 2016; Lim et al., 2017; Thambidurai et al., 2014), inserting functional modification layer (Chen et al., 2008; Wang et al., 2016) or introducing solvent additives (Kyaw et al., 2014) or co-solvent (Zhang et al., 2017), were also employed to improve the excitons dissociation (Zhang et al., 2016), reduce charge recombination (Li et al., 2014) or increase the light absorption (Shi et al., 2017; Yu et al., 2014). Additionally, instead of the regular configuration, PSCs with an inverted structure are usually preferred for efficient operation and better air stability by avoiding using of the low-work-function

metal cathode and the corrosive and hygroscopic poly(3,4-ethylenedioxylenethiophene):poly(styrenesulphonic acid) (PEDOT:PSS) as a hole transport layer, both of which are detrimental to device stability (He et al., 2012; Liu et al., 2013). Alternatively, transition metal oxides (TMOs) such as MoO$_3$ (Cheng et al., 2015), NiO$_x$ (Cheng et al., 2017; Jiang et al., 2015) have widely been used as a hole-transport layer (HTL) to improve the efficiency and stability of PSCs due to its tunable work-function and air stability. Therefore, the less air-sensitive high work function metal anode and metal oxides as carrier transport layer used in the inverted PSCs could apparently inhibit electrode oxidation and prolong cell lifetime (Kyaw et al., 2008; Sun et al., 2011). However, the PCE and stability need further be improved for the viable commercialization of PSCs.

For inverted cells, while a high work function metal is used for the top anode, anode interlayer materials with high work functions are needed to form good Ohmic contacts for enlarging the built-in potential of devices, which is beneficial to reduce the series resistance and increase the carrier extraction (Chen et al., 2012). It is also known that V$_{OC}$ is related to the built-in potential (Luo et al., 2009; Tao et al.,

---

2008), and work function of the positive contact (Brabec, 2004). The previous reports indicated that the oxidation of silver electrode can increase the built-in field at the interface of metal electrode and help to improve hole transport and collection abilities, which can enhance V_{OC} and PCE of cells (Kim et al., 2009). The existence of metal oxide favoring the charge transport was also verified in OELD (Zhang and Wallace, 2008). Furthermore, Berredjem and Morsli et al. demonstrated that the presence of a thin Al_2O_3 layer at the C60/Al interface can greatly increase the shunt resistance and thus improve the open-circuit voltage (Berredjem et al., 2008; Morsli et al., 2008). The AlO_x formation at the interface between photoactive layer and Al electrode is effective to improve PCE of cells due to the enhanced built-in potential (Kim et al., 2012; Zhang et al., 2009). However, the series resistance of cells can be obviously increased for too thick metal oxidation layer, which result in the quick deterioration of cells due to its insulation property (Shi et al., 2013; Singh et al., 2006). Although Al as an efficient electrode for PSCs has been widely applied, there are few care whether Al is a right electrode in PSCs for longtime stability.

In this paper, we compared the performance and air stability of PSCs with Al and AgAl electrodes. PSCs with Al electrode can be limited for longtime application because the thickness of AlO_x self-formed at the MoO_3/Al interface can be continuously increased with aging time. The accurately formed thickness of AlO_x interlayer is important to realize the longtime stability of PSCs and AgAl electrode instead of Al can meet this function. However, the formation of AlO_x process for AgAl electrode can also greatly affect the stability of PSCs. In the meantime, using AZO instead of ZnO as an electron transport layer (ETL) can reach 10.2% of PCE for PSCs.

2. Experimental details

PSCs, with an inverted structure of ITO/ETL/PTB7-Th:PC_{71}BM/ MoO_3/Anode, were fabricated. The pre-patterned indium tin oxide (ITO)/Glass substrates ($10\,\Omega/\square$) were cleaned sequentially with detergent, de-ionized water, acetone and isopropyl alcohol in an ultrasonic bath for 20 min each, and then blow-dried by pure nitrogen gas. After being heat dried in an oven, ITO/Glass substrates were treated with ultraviolet ozone for 15 min. The sol-gel ZnO nanoparticles were synthesized following the procedures described in the previous publications (Lu et al., 2015; Shao et al., 2013). The typical synthesis, a stoichiometric amount of tetramethyl-ammonium hydroxide dissolved in ethanol (0.5 M) was gradually dropped into 0.1 M zinc acetate dihydrate dissolved in dimethyl sulfoxide (DMSO), followed by stirring for an hour at room temperature. After being washed with hexane and ethanol (2:1) mixing solvents, ZnO nanoparticles were dispersed in ethanol. The AZO nanoparticles were synthesized with a modified method according to the published literatures (Alam and Cameron, 2001; Stubhan et al., 2013). In details, Zinc acetate ($Zn(CH_3CO_2)_2\cdot 2H_2O$) and aluminum nitrate ($Al(NO_3)_3\cdot 9H_2O$) were mixed together and dissolved in ethanol. The solution was stirred at 80 °C for 3 h to get a clear solution. The fabrication progress of AZO thin film is the same as that of ZnO layer. Then sol-gel ZnO solutions were spin coated at 4000 rpm for 50 s onto ITO to form 20 nm films, followed by annealing at 150 °C for 30 min in air. PTB7-Th (99%) was purchased from 1-Material INC. and PC_{71}BM (99.5%) was purchased from Solenne BV. An 80 nm thick active layer was deposited on ZnO surface using a blend solution containing PTB7-Th:PC_{71}BM (7 mg/mL:10.5 mg/mL) dissolved in chlorobenzene/1,8-diiodooctane (97:3, v/v) at 1000 rpm for 15 s in argon-filled glove box. A 7 nm thick MoO_3 interlayer and a 100 nm thick Al or AgAl film were then deposited by thermal evaporation at the rate of 0.3 Å/s and 5 or 10 Å/s respectively on the PTB7-Th:PC_{71}BM active layer with base pressure of 3×10^{-4} Pa. A mask with an aperture area of 0.09 cm^2 was used for the current density-voltage (J-V) characteristic measurement to avoid the edge effect. The PSCs without encapsulation were stored in a 10% RH chamber in air.

The J-V characteristics of PSCs were measured by a Keithley 2440

Sourcemeter together with a Newport solar simulator with an AM1.5G illumination of 100 mW/cm^2 calibrated with a standard silicon reference cell. The incident photon to current conversion efficiency (IPCE) of PSCs was measured over the wavelength range from 300 nm to 800 nm using a Newport Optical Power Meter 2936-R and was recorded using TracQ Basic software. The dark J-V characteristics of the cells were measured using an electrochemical workstation (AUTOLAB PGSTAT302N). The absorption spectra of cells with Al electrode were measured using a UV/Vis spectrophotometer (Hitachi U-3900). X-ray photoelectron spectroscopy (XPS) measurements were carried out using an Imageing Photoelectron Spectrometer (Axis Ultra, Kratos Analytical Ltd.) with a monochromatic Al Ka X-ray source. The UV-light illumination was conducted over the wavelength of 365 nm under two 18 W U-type lamp tubes.

3. Results and discussion

3.1. Performance of Al-based inverted PSCs

To investigate the performance variance of Al electrode based PSCs during the aging process, we fabricated a set of inverted PSCs with the structure of ITO/ZnO/PTB7-Th:PC_{71}BM/MoO_3/Al. Fig. 1a shows the J-V characteristics of Al based cells with different aging time. The average parameters and the standard deviations counting eight devices aging for different time are summarized in Table 1. The V_{OC} and FF of the original PSCs were only 0.695 V and 42.1% respectively, which results in the low PCE of 4.8%. The performance of PSCs were obviously increased aging for 16 h in RH 10% at ambient atmosphere condition and got 0.774 V of V_{OC}, 59.5% of FF and 7.3% of PCE respectively. The highest PCE of PSCs was obtained after aging for 36 h, and V_{OC} and FF values of cells were further increased to 0.784 V and 63.0% respectively, which got the highest PCE of 7.8%. The gradually increased V_{OC} and FF of PSCs are attributed to the gradual formation of AlO_x at the interface of Al/MoO_3 due to the oxygen invasion (Berredjem et al., 2008; Morsli et al., 2008), which helps to reduce the contact potential and carrier recombination. The obviously reduced reversed dark current and R_S, and the increased R_{SH} of cells after aging for 16 h and 36 h compared to the original cells further support this conclusion (Kim et al., 2005; Luo et al., 2009), as shown in Fig. 1b and Table 1.

However, as shown in Fig. 1d, the gradually self-formed AlO_x interlayer at the Al/MoO_3 interface can reduce the reflectivity of Al electrode, which would decrease the absorption of the photoactive layer because of the limited thickness of the photoactive layer. The slightly reduced photocurrent and IPCE values of cells aging for 16 h and 36 h compared to the original cells is consistent with this trend, as shown in Fig. 1c and Table 1. Fortunately, the enhanced V_{OC} and FF can easily offset the reduced photocurrent, indicating that the optimal thickness of AlO_x at the interface of Al/MoO_3 can be gradually formed after cells are exposed to air with the right time, which can get superior performance of PSCs. However, the AlO_x thickness can easily further increase with increasing time of cells exposed to air because accurately controlling thickness of AlO_x film at the Al film surface is impossible due to the easy oxidization of Al metal. The too thick AlO_x film can greatly increase the series resistance of cells due to the insulation property of AlO_x, which would accelerate the deterioration of Al electrode based PSCs. Therefore, the optimal and easily controlling AlO_x interlayer at the Al/MoO_3 interface is important to improve the PCE and stability of PSCs.

3.2. Effect of AgAl alloy electrode on the performance of PSCs

To suppress the continuous growth of AlO_x interlayer at the Al electrode surface, the AgAl alloy (3 wt% Al) was introduced as metal electrode of PSCs (Jia et al., 2016; Jiang et al., 2016). Fig. 2 shows the X-ray photoelectron spectroscopy (XPS) spectra of AgAl alloy film. The main element characteristic peaks of Ag 3d5/2, 3d3/2 and O1s are
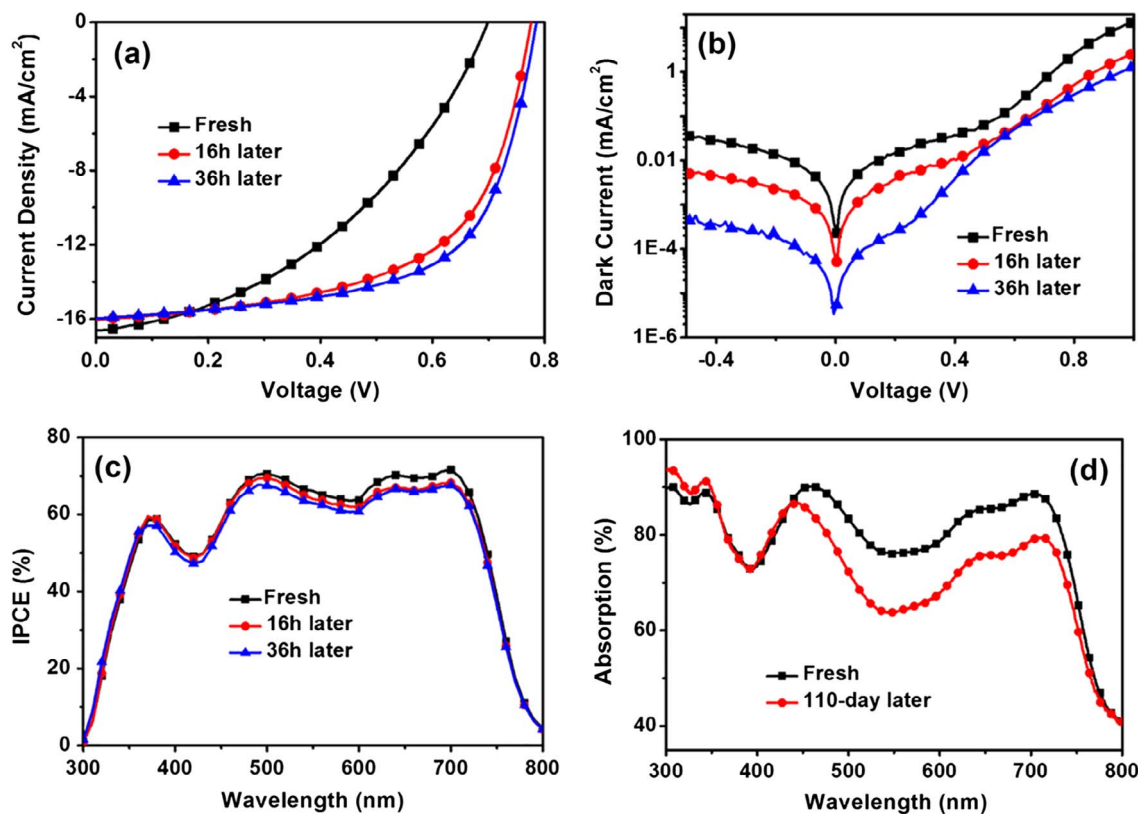
Fig. 1. (a) *J-V* characteristics under 100 mW/cm^2 AM 1.5G simulated solar illuminations, (b) dark *J-V* curves, (c) IPCE spectra and (d) absorption spectra of PSCs (ITO/ZnO/PTB7-Th:PC$_{71}$BM/MoO$_3$/Al) with different aging time.

Table 1
Performance of PSCs with the structure of ITO/ZnO/PTB7-Th:PC$_{71}$BM/MoO$_3$/Al.

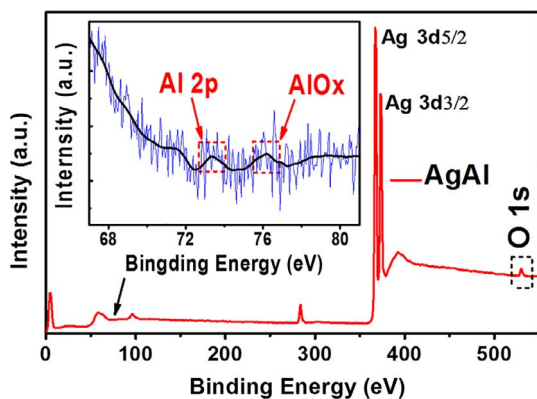| Anode	Time	V_{OC} (V)	J_{SC} (mA/cm^2)	FF (%)	R_S (Ω cm^2)	R_{SH} (Ω cm^2)	PCE (%)
Al	Fresh	0.695	16.6	42.1	119.8	2415.8	4.8 ± 0.06
	16 h later	0.774	16.0	59.5	53.5	3971.2	7.3 ± 0.08
	36 h later	0.784	15.9	63.0	54.1	4381.6	7.8 ± 0.08

Fig. 2. XPS spectra of AgAl alloy film. Inset image shows the core line spectra of Al 2p and AlO$_x$.

vividly clear, and the theoretic position of Al 2p peak is also pointed out. The typical core lines of the Al 2p and AlO$_x$ can be observed for the AgAl film, which are corresponding to the very weak peaks at 72.7 and 76.0 eV respectively due to the low content of Al, as illustrated in the inset of Fig. 2. This is because the Al element of AgAl alloy can be easily oxidized into AlO$_x$ during the thermal evaporation and aging process because Al is an active element. It is known that the Al atom

distribution is inhomogeneous across AgAl films and the rich AlO$_x$ can be self-formed at the interface of AgAl/MoO$_3$ (Jiang et al., 2016; Sugawara et al., 2007). Therefore, the thickness of the interfacial AlO$_x$ interlayer can be controlled due to the limited Al content at the surface of AgAl.

To explore the effect of formation process of AlO$_x$ interlayer on the performance of PSCs, we fabricated two sets of cells with the structure of ITO/ZnO/PTB7-Th:PC$_{71}$BM/MoO$_3$/AgAl under different base pressure. Fig. 3a and c show the *J-V* characteristics of PSCs with the base pressure of 3×10^{-4} Pa and 2×10^{-3} Pa and the corresponding parameters are summarized in Table 2. PSCs based on AgAl electrode evaporated under the base pressure of 2×10^{-3} Pa show inferior performance with PCE of 6.0%, V_{OC} of 0.728 V and FF of 44.3%. The PCE of PSCs was increased to 8.4% due to the greatly enhanced V_{OC} and FF aging for one day. Then, the PCEs of PSCs were quickly decreased to 7.8% and 6.9% respectively aging for 2 and 4 days due to the reduced FF and J_{SC}. However, PSCs based on AgAl electrode evaporated under the base pressure of 3×10^{-4} Pa show superior performance with PCE of 9.2%, V_{OC} of 0.774 V and FF of 64.4%. Furthermore, its PCE show better stability and still keep 9.2% and 9.1% respectively aging for 2 and 4 days. The inferior performance of PSCs evaporated with the low pressure of 2×10^{-3} Pa were further supported by the dark *J-V* curves (Fig. 3b and d). The obviously higher reversed saturation current and lower rectification ratio of PSCs evaporated with the base pressure of 2×10^{-3} Pa compared to 3×10^{-4} Pa indicate the high carrier
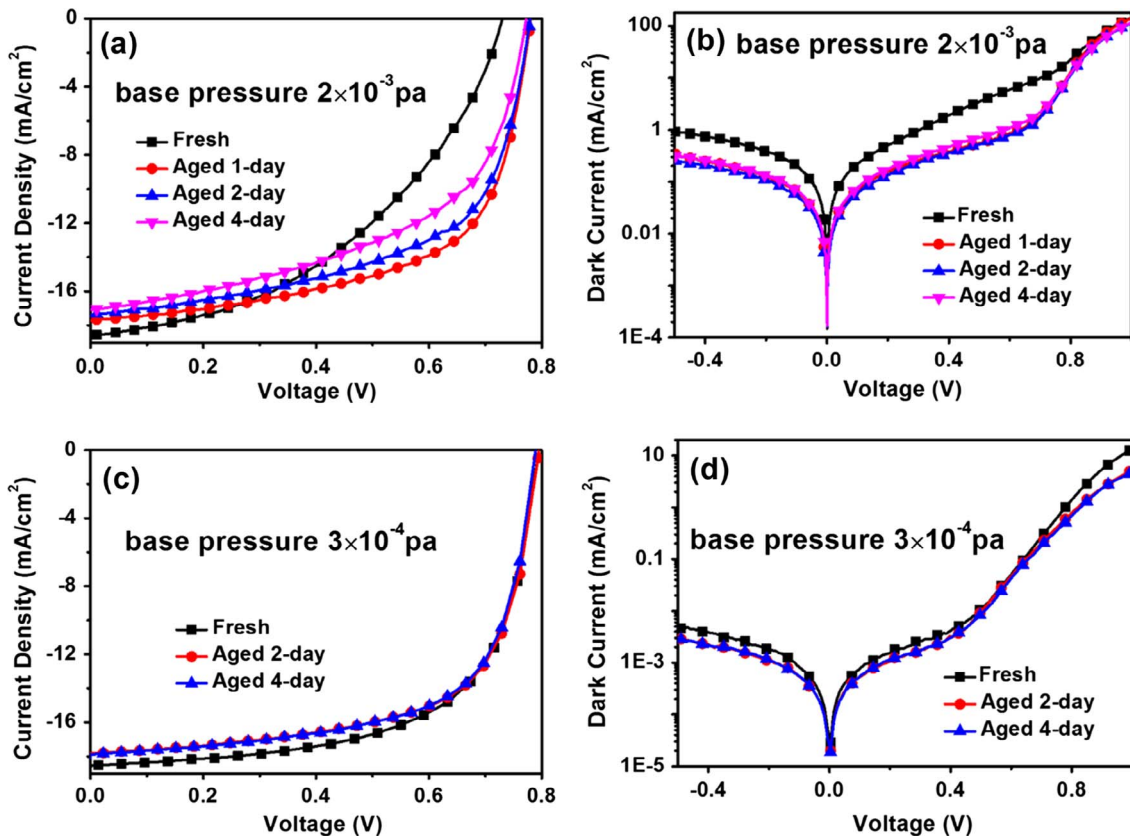
Fig. 3. (a) *J-V* characteristics and (b) dark *J-V* curves of cells evaporated under the base pressure of 2×10^{-3} Pa. (c) *J-V* characteristics and (d) dark *J-V* curves of PSCs evaporated under the base pressure of 3×10^{-4} Pa.

Table 2
Photovoltaic parameters of PSCs under different base pressure with the structure of ITO/ZnO/PTB7-Th:$PC_{71}BM$/MoO_3/AgAl.

Pressure	Time	V_{OC} (V)	J_{SC} (mA/cm^2)	FF (%)	R_S (Ω cm^2)	PCE (%)
2×10^{-3} Pa	Fresh	0.728	18.6	44.3	77.0	6.0 ± 0.04
	1-day	0.779	17.7	61.1	34.3	8.4 ± 0.03
	2-day	0.779	17.4	58.3	38.9	7.8 ± 0.06
	4-day	0.772	17.0	52.6	48.5	6.9 ± 0.02
3×10^{-4} Pa	Fresh	0.774	18.4	64.4	30.4	9.2 ± 0.05
	2-day	0.794	17.7	65.2	10.1	9.2 ± 0.02
	4-day	0.789	17.8	65.1	10.1	9.1 ± 0.07

recombination and inferior carrier transport and collect abilities. Although the reversed saturation current and rectification ratio of PSCs with 2×10^{-3} Pa have been improved aging for one day, the electrical properties of cells are still inferior compared to cells with 3×10^{-4} Pa. The obvious difference of dark *J-V* curves for the initial PSCs with 2×10^{-3} Pa compared to aging for 1 day indicates that the interface between MoO_3/AgAl is unstable. This is because the rough and porous AlO_x interlayer may be formed under severe participation of too much residual oxygen in the vacuum chamber. However, the dense and thin AlO_x interlayer can be formed under the little residual oxygen at the ideal vacuum pressure, which can greatly improve the performance and stability of PSCs.

Fig. 4 shows the decay performance parameters of inverted PSCs (ITO/ZnO/PTB7-Th:$PC_{71}BM$/MoO_3/Anode) with the aging time. AgAl and Al electrodes were thermally evaporated under the based pressure of 3×10^{-4} Pa. AgAl-based cells still remained 69% of its original PCE values and got 6.5% of PCE after aging for 796 days. Al based PSCs with ZnO ETL can reach the highest PCE of 7.8% after aging for 36 h, which was acted as a reference value of cells. Al based PSCs was dropped to

3.7% of PCE and only remained 47% of the initial PCE value aging for 796 days. The obviously low J_{SC} of cells with Al compared to AgAl electrode is attributed to the low reflectivity of Al electrode, which decreases the light absorption of the active layer (Jia et al., 2016; Kim et al., 2006). The V_{OC} and FF values of PSCs with AgAl and Al electrodes are almost similar at the initial stage. However, the V_{OC} and FF values of cells with Al electrode were obviously lower than that of cells with AgAl electrode aging for 194 and 796 days, which is roughly consistent with the synchronously increased R_S value of Al based cells, indicating that the deterioration interface of Al/MoO_3 is primarily responsible for the decay of cells due to too thick AlO_x formation. Therefore, it is important for cells to keep longtime stability for the metal oxidation interlayer between MoO_3 and metal electrode (such as using AgAl) to improve the stability of PSCs.

Fig. 5 shows the energy level structure diagrams of cells with Al and AgAl anode. The work functions of Al and AgAl measured with Test Instrument of Surface Work Function are 4.3 eV and 4.7 eV, respectively. The work functions of MoO_3 is sensitive to the exposed condition and is reduced when MoO_3 layer is diffused into with metal atoms (Al or Ag) or/and exposed to oxygen, which favors hole transport and ex-action (Liu et al., 2012). The self-formed AlO_x at the metal electrode makes the interface of MoO_x/AgAl or Al form the depleted region, which can greatly increase holes tunnel from MoO_x to metal electrode. However, the carrier tunneling probability is closely related to the AlO_x thickness, and the thin and dense thickness of insulator helps to greatly increase tunneling probability (Zhang et al., 2006). The right AlO_x thickness of Al or AgAl electrode can strongly bend the energy band at the interface, as shown in Fig. 5b and c. With further increasing time of Al based cells exposed to air, the thicker AlO_x thickness would be formed and decreased the tunneling probability due to the easy oxidization of Al metal, as shown in Fig. 5d. Therefore, the accurately controlling thickness of AlO_x interlayer for AgAl have superior longtime
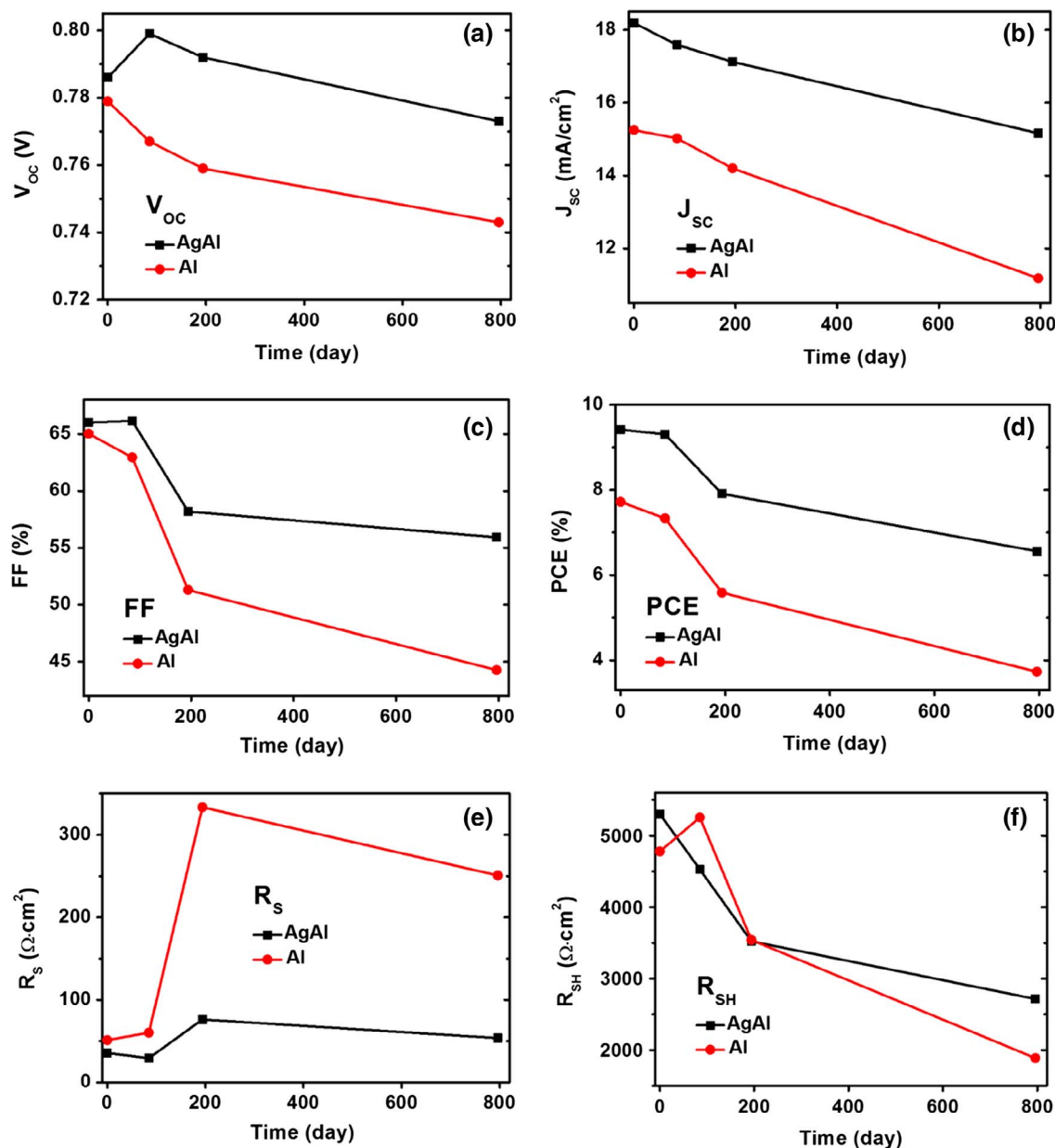
Fig. 4. (a) Open-circuit voltage, (b) short-circuit current, (c) fill factor, (d) power conversion efficiency, (e) series resistance and (f) shunt resistance of inverted PSCs as a function of the aging time.

stability of PSCs compared to PSCs of Al electrode.

3.3. Effect of AZO on the performance of PSCs

AZO compared with ZnO ETL has better electrical and morphology properties, which are conducive to improve the performance of inverted PSCs (Aprilia et al., 2013; Liu et al., 2016; Yu et al., 2017). Therefore, PSCs with AZO electron transport layer and AgAl electrode evaporated with the pressure of 3×10^{-4} Pa were fabricated. Fig. 6 shows the *J-V* characteristics of AgAl based PSCs with ZnO and AZO electron transport layers respectively. Table 3 lists the average values of the cell parameters and their standard deviations aging for different time. Compared with the PCE (9.3%) of cells with ZnO layer, the highest PCE of AZO-based PSCs is up to 10.2% via improving short-circuit photocurrent density from 17.4 to 18.5 mA/cm^2 and fill factor from 67.8% to 70.0% due to the increased carrier concentration and conductivity (Tsai et al., 2013). PSCs still remain 87% and 85% of the initial PCE values for AZO and ZnO layer respectively aging for

120 days in RH 10%, as shown in Fig. 7, indicating that PSCs with AZO ETL exhibit slightly better long-term stability. However, PSCs with ZnO layer show quick deterioration under UV light illumination, and PCE of cells was decreased to 27% of the initial PCE value exposed for 29 h. While PCE of cells with AZO still keep 53% of the initial PCE aging for 29 h under UV illumination, the greatly enhanced photo-stability is mainly attributed to the reduced defect states of Zn ions because aluminum is filled in Zn vacancies, and therefore the decreased amount of adsorbed oxygen molecules (Lin et al., 2016; Prosa et al., 2016).

4. Conclusions

The performance and stability of inverted PSCs with Al and AgAl electrodes were investigated. The PCE of PSCs with Al electrode can be gradually improved and reach the highest value aging for 36 h. PSCs with AgAl electrode can be reached the highest PCE value without aging. Furthermore, PSCs with AgAl electrode still got 6.6% of PCE and retained 69% of the initial PCE value aging for 796 days, showing
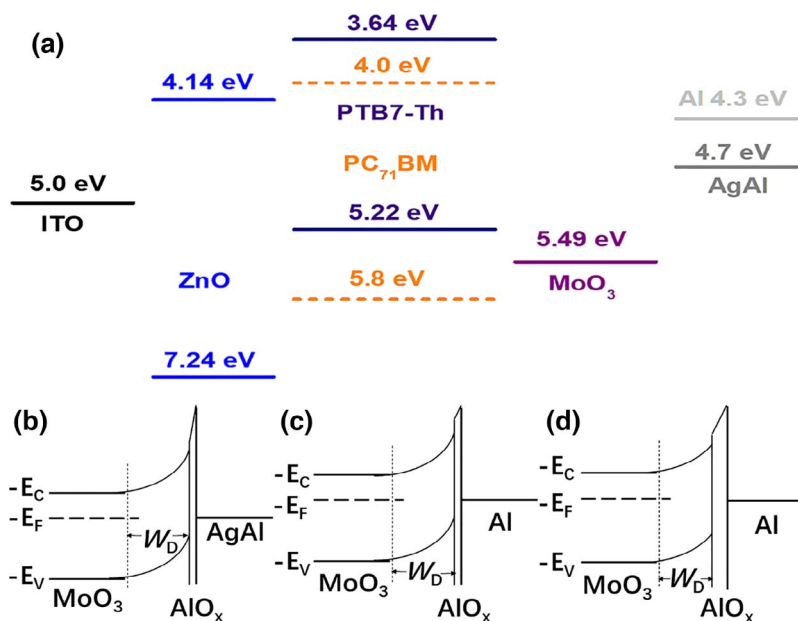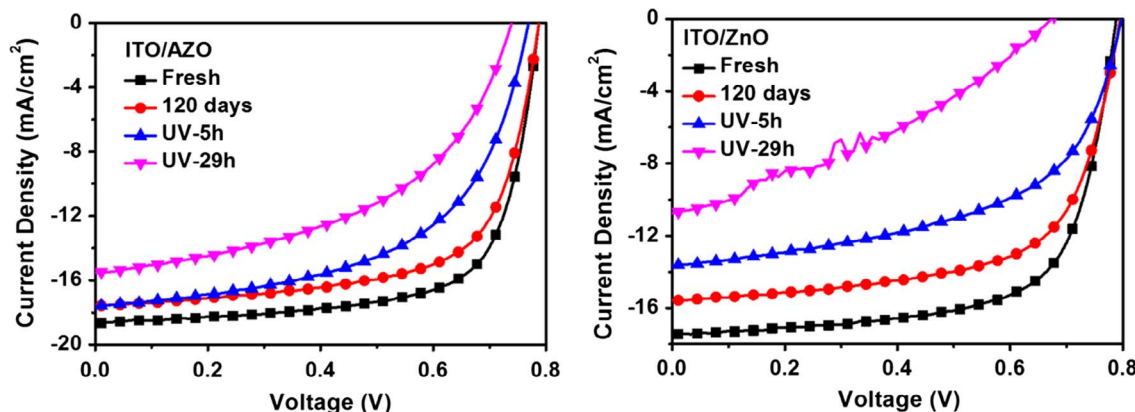
Fig. 6. *J-V* characteristics of AgAl based PSCs with AZO and ZnO electron transport layer under AM 1.5G illumination of 100 mW/cm².

Table 3
Photovoltaic performance of AgAl based PSCs with ZnO and AZO layer.

ETL	Time	V_{OC} (V)	J_{SC} (mA/cm²)	FF (%)	R_S (Ω cm²)	PCE (%)
AZO	Fresh	0.788	18.5	70.0	31.2	10.2 ± 0.04
ZnO	Fresh	0.788	17.4	67.8	37.6	9.3 ± 0.02
AZO	120 days	0.787	17.2	66.2	35.0	8.9 ± 0.05
ZnO	120 days	0.791	15.7	63.7	52.2	7.9 ± 0.03
AZO	UV-5 h	0.764	17.5	55.0	54.0	7.3 ± 0.09
ZnO	UV-5 h	0.793	14.3	51.3	73.2	5.8 ± 0.01
AZO	UV-29 h	0.730	15.6	47.5	89.3	5.4 ± 0.01
ZnO	UV-29 h	0.670	10.8	34.0	261.4	2.4 ± 0.07

Fig. 7. Normalized PCE of PSCs as a function of aging time and UV illumination. Cells were exposed to UV illumination after aging for 120 days (2880 h) in RH 10%.

amazing stability. However, PSCs with Al electrode was dropped to 3.7% of PCE aging for 796 days. The enhanced stability of PSCs with AgAl electrode is attributed to the dense and limited AlO_x thickness at the MoO_3/AgAl interface due to the low content of Al in AgAl alloy. PSCs with AZO ETL and AgAl electrode can obviously improve PCE and reach 10.2%, and furthermore have better UV resistance compared to PSCs with ZnO layer. In summary, Al as an electrode for PSCs is limited for realizing longtime stability due to the continuously increased thickness of AlO_x interlayer. The dense and limited thickness of AlO_x self-formed at the interface between the carrier transport layer and AgAl electrode is important to realize longtime stability of PSCs. The Ag alloy electrode, such as AgAl alloy, is a good strategy to accurately
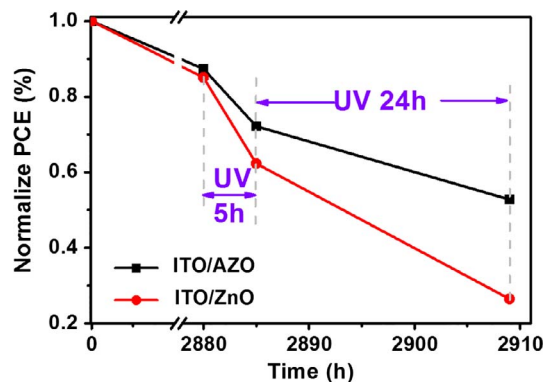
control the thickness of the metal oxidation interlayer between the carrier transport layer and metal electrode, which is beneficial to improve the longtime stability of devices.

References

Alam, M.J., Cameron, D.C., 2001. Preparation and properties of transparent conductive aluminum-doped zinc oxide thin films by sol–gel process. J. Vac. Sci. Technol. A. 19, 1642–1646.

An, Q., Zhang, F., Zhang, J., Tang, W., Wang, Z., Li, L., Xu, Z., Teng, F., Wang, Y., 2013. Enhanced performance of polymer solar cells through sensitization by a narrow band gap polymer. Sol. Energy Mater. Sol. Cells 118, 30–35.

Aprilia, A., Wulandari, P., Suendo, V., Herman, Hidayat, R., Fujii, A., Ozaki, M., 2013. Influences of dopant concentration in sol–gel derived AZO layer on the performance of P3HT:PCBM based inverted solar cell. Sol. Energy Mater. Sol. Cells 111, 181–188.

Berredjem, Y., Karst, N., Cattin, L., Lakhdartoumi, A., Godoy, A., Soto, G.M., Diaz, F.R., Valle, M.A.D., Morsli, M., Drici, A., 2008. The open circuit voltage of encapsulated plastic photovoltaic cells. Dyes Pigm. 78, 148–156.

Brabec, C.J., 2004. Organic photovoltaics: technology and market. Sol. Energy Mater. Sol. Cells 83, 273–292.

Chen, S., Manders, J.R., Tsang, S., So, F., 2012. Metal oxides for interface engineering in polymer solar cells. J. Mater. Chem. 22, 24202–24212.

Chen, X., Zhao, C., Rothberg, L., Ng, M.-K., 2008. Plasmon enhancement of bulk heterojunction organic photovoltaic devices by electrode modification. Appl. Phys. Lett. 93, 123302.

Cheng, J., Ren, X., Zhu, H.L., Mao, J., Liang, C., Zhuang, J., Roy, V.A.L., Choy, W.C.H., 2017. Pre- and post-treatments free nanocomposite based hole transport layer for high performance organic solar cells with considerably enhanced reproducibility. Nano Energy 34, 76–85.

Cheng, J., Xie, F., Liu, Y., Sha, W.E.I., Li, X., Yang, Y., Choy, W.C.H., 2015. Efficient hole transport layers with widely tunable work function for deep HOMO level organic solar cells. J. Mater. Chem. A. 3, 23955–23963.

He, Z., Zhong, C., Su, S., Xu, M., Wu, H., Cao, Y., 2012. Enhanced power-conversion efficiency in polymer solar cells using an inverted device structure. Nat. Photon. 6, 593–597.

Huang, J., Gu, Z., Zuo, L., Ye, T., Chen, H., 2016. Morphology control of planar heterojunction perovskite solar cells with fluorinated PDI films as organic electron transport layer. Sol. Energy 133, 331–338.

Jia, X., Jiang, Z., Chen, X., Zhou, J., Pan, L., Zhu, F., Sun, Z., Huang, S., 2016. Highly efficient and air stable inverted polymer solar cells using LiF-modified ITO cathode and MoO3/AgAl alloy anode. ACS Appl. Mater. Interfaces 8, 3792–3799.

Jiang, F., Choy, W.C.H., Li, X., Zhang, D., Cheng, J., 2015. Post-treatment-free solution-processed non-stoichiometric NiOx nanoparticles for efficient hole-transport layers of organic optoelectronic devices. Adv. Mater. 27, 2930–2937.

Jiang, Z., Chen, X., Lin, X., Jia, X., Wang, J., Pan, L., Huang, S., Zhu, F., Sun, Z., 2016. Amazing stable open-circuit voltage in perovskite solar cells using AgAl alloy electrode. Sol. Energy Mater. Sol. Cells 146, 35–43.

Kim, J., Kim, J., Kwak, S., Yu, J., Jang, Y., Jo, J., Lee, T., Kim, I., 2012. Effects of the Al cathode evaporation rate on the performance of organic solar cells. Appl. Phys. Lett. 101, 213304.

Kim, J., Na, S., Ha, G., Kwon, M., Park, I., Lim, J., Park, S., Kim, M., Choi, D., Min, K., 2006. Thermally stable and highly reflective AgAl alloy for enhancing light extraction efficiency in GaN light-emitting diodes. Appl. Phys. Lett. 88, 043507–043509.

Kim, J.B., Kim, C.S., Kim, Y.S., Loo, Y.-L., 2009. Oxidation of silver electrodes induces transition from conventional to inverted photovoltaic characteristics in polymer solar cells. Appl. Phys. Lett. 95, 183301–183303.

Kim, Y., Choulis, S.A., Nelson, J., Bradley, D.D.C., Cook, S., Durrant, J.R., 2005. Device annealing effect in organic solar cells with blends of regioregular poly(3-hexylthiophene) and soluble fullerene. Appl. Phys. Lett. 86, 063502–063504.

Kyaw, A.K.K., Sun, X.W., Jiang, C.Y., Lo, G., Zhao, D.W., Kwong, D.L., 2008. An inverted organic solar cell employing a sol-gel derived ZnO electron selective layer and thermal evaporated MoO3 hole selective layer. Appl. Phys. Lett. 93, 221107.

Kyaw, A.K.K., Wang, D.H., Luo, C., Cao, Y., Nguyen, T.-Q., Bazan, G.C., Heeger, A.J., 2014. Effects of solvent additives on morphology, charge generation, transport, and recombination in solution-processed small-molecule solar cells. Adv. Energy Mater. 4, 1301469.

Li, C., Chang, C., Zang, Y., Ju, H., Chueh, C., Liang, P., Cho, N., Ginger, D.S., Jen, A.K.Y., 2014. Suppressed charge recombination in inverted organic photovoltaics via enhanced charge extraction by using a conductive fullerene electron transport layer. Adv. Mater. 26, 6262–6267.

Liao, S., Jhuo, H., Cheng, Y., Chen, S., 2013. Fullerene derivative-doped zinc oxide nanofilm as the cathode of inverted polymer solar cells with low-bandgap polymer (PTB7-Th) for high performance. Adv. Mater. 25, 4766–4771.

Lim, J.W., Hwang, D.K., Lim, K.Y., Kang, M., Shin, S.-C., Kim, H.-S., Choi, W.K., Shim, J.W., 2017. ZnO-morphology-dependent effects on the photovoltaic performance for inverted polymer solar cells. Sol. Energy Mater. Sol. Cells 169, 28–32.

Lin, X., Luo, H., Jia, X., Wang, J., Zhou, J., Jiang, Z., Pan, L., Huang, S., Chen, X., 2016. Efficient and ultraviolet durable inverted polymer solar cells using thermal stable GZO-AgTi-GZO multilayers as a transparent electrode. Org. Electron. 39, 177–183.

Liu, C., Yi, C., Wang, K., Yang, Y., Bhatta, R.S., Tsige, M., Xiao, S., Gong, X., 2015. Single-junction polymer solar cells with over 10% efficiency by a novel two-dimensional donor-acceptor conjugated copolymer. ACS Appl. Mater. Interfaces 7, 4928–4935.

Liu, H., Wu, Z., Hu, J., Song, Q., Wu, B., Lam Tam, H., Yang, Q., Hong Choi, W., Zhu, F., 2013. Efficient and ultraviolet durable inverted organic solar cells based on an aluminum-doped zinc oxide transparent cathode. Appl. Phys. Lett. 103, 043309.

Liu, J., Shao, S., Fang, G., Meng, B., Xie, Z., Wang, L., 2012. High-efficiency inverted polymer solar cells with transparent and work-function tunable MoO3-Al composite film as cathode buffer layer. Adv. Mater. 24, 2774–2779.

Liu, X., Li, X., Li, Y., Song, C., Zhu, L., Zhang, W., Wang, H., Fang, J., 2016. High-performance polymer solar cells with PCE of 10.42% via Al-doped ZnO cathode interlayer. Adv. Mater. 28, 7405–7412.

Lu, Z., Chen, X., Zhou, J., Jiang, Z., Huang, S., Zhu, F., Piao, X., Sun, Z., 2015. Performance enhancement in inverted polymer solar cells incorporating ultrathin Au and LiF modified ZnO electron transporting interlayer. Org. Electron. 17, 364–370.

Luo, J., Wu, H., He, C., Li, A., Yang, W., Cao, Y., 2009. Enhanced open-circuit voltage in polymer solar cells. Appl. Phys. Lett. 95, 043301.

Morsli, M., Berredjem, Y., Drici, A., Kouskoussa, B., Boulmokh, A., Bernede, J.C., 2008. Influence of Alq3 and/or Al$_2$O$_3$ layers at the C60/aluminum interface on the I–V characteristics of CuPc/C60-based solar cells. Phys. Stat. Solidi A 205, 1226–1232.

Prosa, M., Tessarolo, M., Bolognesi, M., Margeat, O., Gedefaw, D., Gaceur, M., Videlotackermann, C., Andersson, M.R., Muccini, M., Seri, M., 2016. Enhanced ultraviolet stability of air-processed polymer solar cells by Al doping of the ZnO interlayer. ACS Appl. Mater. Interfaces 8, 1635–1643.

Shao, S., Zheng, K., Pullerits, T., Zhang, F., 2013. Enhanced performance of inverted polymer solar cells by using poly(ethylene oxide)-modified ZnO as an electron transport layer. ACS Appl. Mater. Interfaces 5, 380–385.

Shi, B., Liu, B., Luo, J., Li, Y., Zheng, C., Yao, X., Fan, L., Liang, J., Ding, Y., Wei, C., Zhang, D., Zhao, Y., Zhang, X., 2017. Enhanced light absorption of thin perovskite solar cells using textured substrates. Sol. Energy Mater. Sol. Cells 168, 214–220.

Shi, J.-J., Dong, W., Xu, Y.-Z., Li, C.-H., Lv, S.-T., Zhu, L.-F., Dong, J., Luo, Y.-H., Li, D.-M., Meng, Q.-B., Chen, Q., 2013. Enhanced performance in perovskite organic lead iodide heterojunction solar cells with metal-insulator-semiconductor back contact. Chin. Phys. Lett. 30, 128402.

Singh, V., Parsarathy, B., Singh, R.S., Aguilera, A., Anthony, J.E., Payne, M.M., 2006. Characterization of high-photovoltage CuPc-based solar cell structures. Sol. Energy Mater. Sol. Cells 90, 798–812.

Stubhan, T., Litzov, I., Li, N., Salinas, M., Steidl, M., Sauer, G., Forberich, K., Matt, G.J., Halik, M., Brabec, C.J., 2013. Overcoming interface losses in organic solar cells by applying low temperature, solution processed aluminum-doped zinc oxide electron extraction layers. J. Mater. Chem. 1, 6004–6009.

Sugawara, K., Kawamura, M., Abe, Y., Sasaki, K., 2007. Comparison of the agglomeration behavior of Ag(Al) films and Ag(Au) films. Microelectron. Eng. 84, 2476–2480.

Sun, Y., Takacs, C.J., Cowan, S.R., Seo, J.H., Gong, X., Roy, A., Heeger, A.J., 2011. Efficient, air-stable bulk heterojunction polymer solar cells using MoO(x) as the anode interfacial layer. Adv. Mater. 23, 2226–2230.

Tao, C., Ruan, S., Zhang, X., Xie, G., Shen, L., Kong, X., Dong, W., Liu, C., Chen, W., 2008. Performance improvement of inverted polymer solar cells with different top electrodes by introducing a MoO3 buffer layer. Appl. Phys. Lett. 93, 193307–193309.

Thambidurai, M., Kim, J.Y., Song, J., Ko, Y., Muthukumarasamy, N., Velauthapillai, D., Lee, C., 2014. Nanocrystalline Ga-doped ZnO thin films for inverted polymer solar cells. Sol. Energy 106, 95–101.

Tsai, S., Ho, S.T., Jhuo, H., Ho, C., Chen, S.A., He, J., 2013. Toward high efficiency of inverted organic solar cells: concurrent improvement in optical and electrical properties of electron transport layers. Appl. Phys. Lett. 102, 253111–253116.

Wang, J., Jia, X., Zhou, J., Pan, L., Huang, S., Chen, X., 2016. Improved performance of polymer solar cells by thermal evaporation of AgAl alloy nanostructures into the hole-transport layer. ACS Appl. Mater. Interfaces 8, 26098–26104.

Yu, X., Yu, X., Zhang, J., Hu, Z., Zhao, G., Zhao, Y., 2014. Effective light trapping enhanced near-UV/blue light absorption in inverted polymer solar cells via sol–gel textured Al-doped ZnO buffer layer. Sol. Energy Mater. Sol. Cells 121, 28–34.

Yu, X., Yu, X., Zhang, J., Zhang, D., Chen, L., Long, Y., 2017. Light-trapping Al-doped ZnO thin films for organic solar cells. Sol. Energy 153, 96–103.

Zhang, C., Tong, S.W., Zhu, C., Jiang, C., Kang, E.T., Chan, D.S.H., 2009. Enhancement in open circuit voltage induced by deep interface hole traps in polymer-fullerene bulk heterojunction solar cells. Appl. Phys. Lett. 94, 103305.

Zhang, H.M., Wallace, C.H.C., 2008. Highly efficient organic light-emitting devices with surface-modified metal anode by vanadium pentoxide. J. Phys. D: Appl. Phys. 41, 062003.

Zhang, S.T., Zhou, Y.C., Zhao, J.M., Zhan, Y.Q., Wang, Z.J., Wu, Y., Ding, X.M., Hou, X.Y., 2006. Role of hole playing in improving performance of organic light-emitting devices with an Al$_2$O$_3$ layer inserted at the cathode-organic interface. Appl. Phys. Lett. 89, 043502.

Zhang, W., Shen, H., Guralnick, B.W., Kirby, B.J., Nguyen, N.A., Remy, R., Majkrzak, C.F., Mackay, M.E., 2016. Correlation between morphology and device performance of pBTTT:PC71BM solar cells. Sol. Energy Mater. Sol. Cells 155, 387–396.

Zhang, X., Zheng, D., Xing, S., Wang, H., Huang, J., Yu, J., 2017. Precisely control the morphology and crystallization of temperature-dependent aggregation bulk heterojunction by using co-solvent system for optimized light intensity distribution and its effect on thick active layer polymer solar cells. Sol. Energy 147, 106–112.

Zhao, J., Li, Y., Yang, G., Jiang, K., Lin, H., Ade, H., Ma, W., Yan, H., 2016. Efficient organic solar cells processed from hydrocarbon solvents. Nat. Energy 1, 15027–15034.

Zhao, W., Li, S., Zhang, S., Liu, X., Hou, J., 2017. Ternary polymer solar cells based on two acceptors and one donor for achieving 12.2% efficiency. Adv. Mater. 29, 1604059–1604066.